

Structure of the human Mediator–RNA polymerase II pre-initiation complex

<https://doi.org/10.1038/s41586-021-03555-7>

Received: 26 January 2021

Accepted: 14 April 2021

Published online: 26 April 2021

 Check for updates

Srinivasan Rengachari^{1,2}, Sandra Schilbach^{1,2}, Shintaro Aibara^{1,2}, Christian Dienemann¹ & Patrick Cramer¹✉

Mediator is a conserved coactivator complex that enables the regulated initiation of transcription at eukaryotic genes^{1–3}. Mediator is recruited by transcriptional activators and binds the pre-initiation complex (PIC) to stimulate the phosphorylation of RNA polymerase II (Pol II) and promoter escape^{1–6}. Here we prepare a recombinant version of human Mediator, reconstitute a 50-subunit Mediator–PIC complex and determine the structure of the complex by cryo-electron microscopy. The head module of Mediator contacts the stalk of Pol II and the general transcription factors TFIIB and TFIIE, resembling the Mediator–PIC interactions observed in the corresponding complex in yeast^{7–9}. The metazoan subunits MED27–MED30 associate with exposed regions in MED14 and MED17 to form the proximal part of the Mediator tail module that binds activators. Mediator positions the flexibly linked cyclin-dependent kinase (CDK)-activating kinase of the general transcription factor TFIIH near the linker to the C-terminal repeat domain of Pol II. The Mediator shoulder domain holds the CDK-activating kinase subunit CDK7, whereas the hook domain contacts a CDK7 element that flanks the kinase active site. The shoulder and hook domains reside in the Mediator head and middle modules, respectively, which can move relative to each other and may induce an active conformation of the CDK7 kinase to allosterically stimulate phosphorylation of the C-terminal domain.

Mediator consists of the head, middle and tail modules, which together comprise 21 and 26 subunits in yeast and humans, respectively^{1–3}. Mediator also associates with a four-subunit kinase module that is not part of the Mediator–PIC complex^{10–12}. Structural studies of Mediator were long hampered by its large size and flexibility and therefore concentrated on the yeast complex^{3,13–15}. Detailed structures were obtained for the head module^{16–18}, and a unified subunit architecture of Mediator was derived^{19–21}. The functional core of Mediator includes the head and middle modules^{7,22}. The structure of the core Mediator highlighted that the MED14 subunit has an architectural role²³.

The location of the yeast core Mediator on a PIC that lacks TFIIH was previously determined, and three Mediator–PIC interfaces were defined and named A, B and C⁷. Structural analysis of a yeast Mediator–PIC complex confirmed the location of Mediator and revealed an additional contact between Mediator and a flexibly linked TFIIH module, the CDK-activating kinase (CAK)⁸. CAK contains the kinase subunit CDK7 and two other subunits, cyclin H and MAT1²⁴. The structure of a yeast core Mediator–PIC complex at a resolution of 5.8 Å showed a similar location of the CAK and provided more detailed insights into the Mediator–PIC interfaces⁹. Despite this progress, structures of human Mediator and its complex with the PIC are lacking. It is thus unclear how human Mediator differs from its yeast counterpart and whether human Mediator interacts with the PIC in a conserved manner.

Here we prepared a 20-subunit recombinant version of human Mediator and determined the structure of this Mediator bound to the PIC.

The structure confirms that the core Mediator is conserved and reveals subunits in the proximal part of the tail module and resembles the structure of mouse Mediator. Human Mediator binds the PIC at the same position as its yeast counterpart, but there are also differences in the Mediator–PIC interfaces. We also define the orientation of the CAK module and uncover two interfaces between Mediator and CDK7.

Recombinant human Mediator

Structural studies of human Mediator have thus far relied on scarce and often heterogeneous endogenous preparations. To study human Mediator at a high resolution, we prepared a recombinant version of Mediator after co-expression of its subunits in insect cells (Methods). Initial attempts to use the 15 subunits that are orthologous to those present in the yeast core Mediator²³ did not result in a well-defined preparation. However, when we also co-expressed subunits MED26–MED30, a soluble and pure 20-subunit recombinant human Mediator complex was obtained (Extended Data Fig. 1a). The recombinant human Mediator contains the complete architectural subunit MED14, the head and middle modules and the proximal part of the tail module that binds the head²⁰. The recombinant Mediator lacks subunits MED1, MED15, MED16, MED23, MED24 and MED25, which form the distal part of the tail module that faces away from the PIC⁸. These efforts established a route to obtain milligram quantities of human Mediator for structural studies.

¹Department of Molecular Biology, Max Planck Institute for Biophysical Chemistry, Göttingen, Germany. ²These authors contributed equally: Srinivasan Rengachari, Sandra Schilbach, Shintaro Aibara. ✉e-mail: patrick.cramer@mpibpc.mpg.de

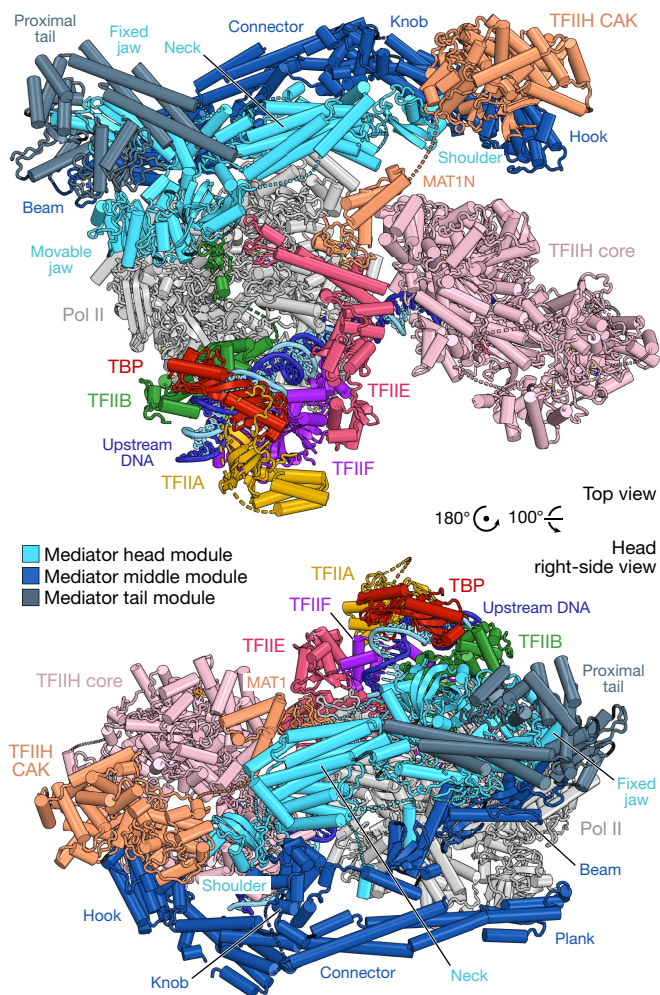


Fig. 1 | Structure of the human Mediator–PIC complex. Two views^{9,37} of the Mediator–PIC structure. The TFIH core and CAK modules are distinguished by colour. Positions of selected TFIH subunits and Mediator domains within the head, middle and tail modules are indicated. The DNA template and non-template strands are in dark and light blue, respectively. Dashed lines represent flexible linkers. The same colour code is used throughout the manuscript.

Structure of the human Mediator–PIC complex

We reconstituted the Mediator–PIC complex using the recombinant human Mediator and the components of an active PIC described in the accompanying paper²⁵—namely, recombinant human general transcription factors TBP, TFIIB, TFIIE, TFIIIF and TFIIH²⁶, and *Sus scrofa domestica* Pol II²⁷, which is 99.9% identical to human Pol II (Methods). We also included ADP–BeF₃, which can act as a transition-state analogue for the catalytic TFIH subunits XPB, XPD and CDK7. The resulting 50-subunit Mediator–PIC complex (Extended Data Fig. 1b) was subjected to single-particle cryo-electron microscopy (cryo-EM) analysis (Extended Data Table 1). We used three-dimensional (3D) classification to identify a subset of particles that contain the complete complex (Extended Data Fig. 2). Particles were observed with closed or open promoter DNA, but good cryo-EM density of Mediator was only obtained for particles that contained closed DNA. The density for Mediator and TFIH was improved by focused classification and with masked refinements. This led to a reconstruction of the Mediator–PIC assembly at an overall resolution of 4.5 Å, with a local resolution of around 3.5 Å for Pol II and the Mediator head module (Extended Data Figs. 2–4).

To derive a model for the human Mediator–PIC complex, we first placed our PIC structure in the closed promoter state²⁵ and then fitted the RPB4–RPB7 stalk and parts of TFIIE into the cryo-EM density map (Methods). The remaining unaccounted density was interpreted in four steps. First, the well-defined density for the Mediator head module allowed for manual rebuilding of a homology model based on the structure of the yeast core Mediator²³. Second, the density for the Mediator middle module showed secondary structure and enabled unambiguous rigid-body fitting of a homology model derived from the structure of the yeast core Mediator²³. Third, unaccounted densities at one end of the Mediator core could be assigned to the Mediator subunits MED27–MED30 and modelled de novo. The last remaining density was unambiguously fitted with the CDK7–cyclin H–MAT1 structure²⁸. The resulting structure lacks only MED26 and shows good stereochemistry (Extended Data Table 1).

The overall structure of the human Mediator–PIC complex resembles its yeast counterpart, highlighting the high conservation of the general transcription initiation machinery throughout eukaryotes (Fig. 1, Supplementary Video 1). Human Mediator interacts with the core PIC around the RPB4–RPB7 stalk of Pol II via its head module. Human Mediator occupies the same location on the PIC and adopts the same

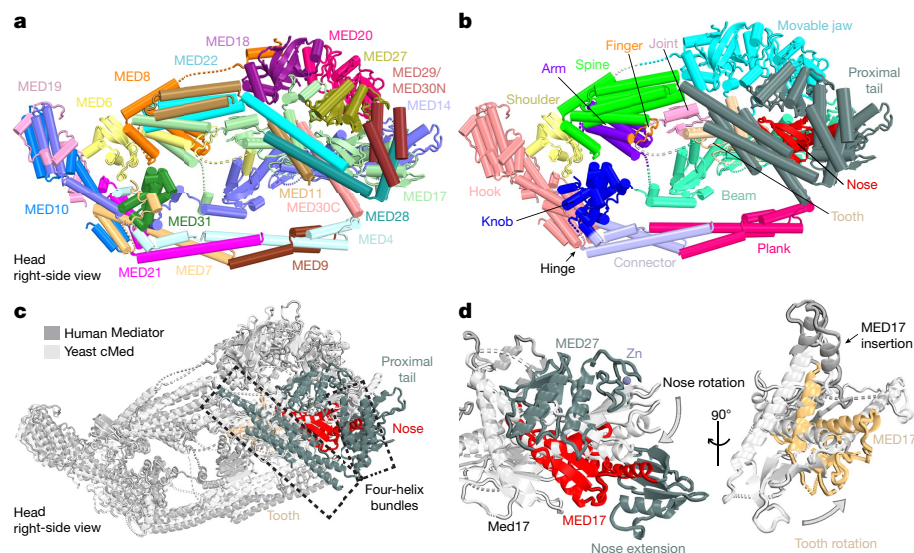


Fig. 2 | Features of the structure of human Mediator. **a**, Subunit architecture. Subunits are shown in different colours. **b**, Domain architecture. Domains are shown in different colours. **c**, Comparison with the structure of the core Mediator (cMed) from *Schizosaccharomyces pombe* (white). Altered MED17 regions and the proximal tail are highlighted. **d**, Alterations in human MED17 compared with its yeast counterpart (white).

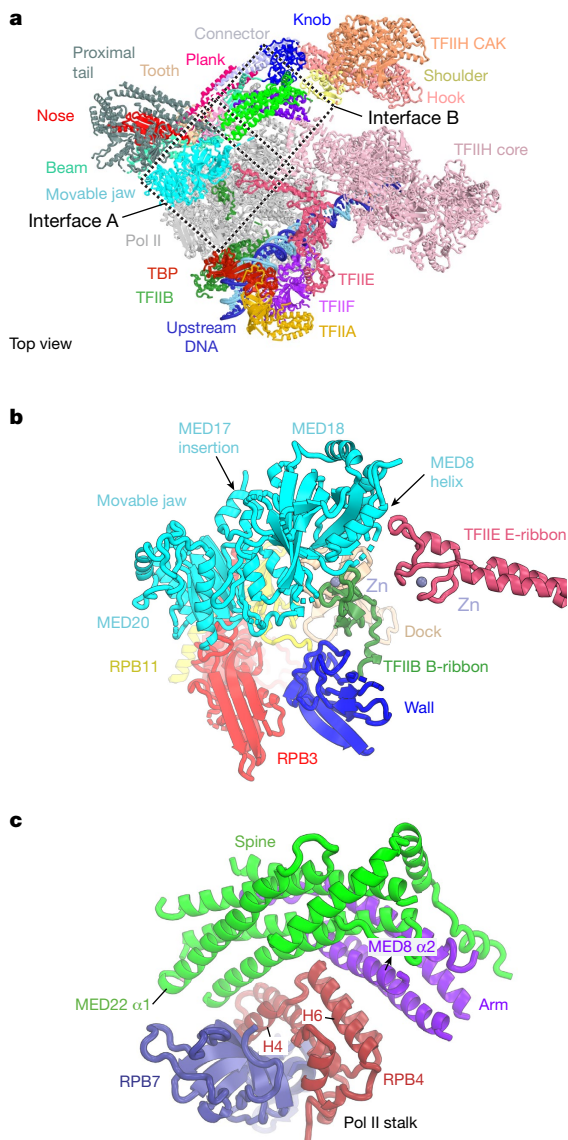


Fig. 3 | Interactions between Mediator and the core PIC. **a**, Structure of the human Mediator–PIC complex with the domains of Mediator coloured as in Fig. 2b. The location of the Mediator–PIC interfaces A and B are indicated (black dotted lines). **b**, Magnified view of Interface A. Interface A involves interactions between the ‘movable jaw’ submodule of the Mediator head domain, the TFIIB B-ribbon and the TFIIE E-ribbon. **c**, Magnified view of Interface B. Interface B involves interactions between the ‘neck’ submodule of the Mediator head domain and the Pol II RPB4–RPB7 stalk.

overall orientation as observed in the structure of the yeast Mediator–PIC complex^{7–9}. Mediator binding does not alter PIC structure²⁵, except for a change in the relative orientation of the Pol II stalk and the TFIIE domain ‘E-ribbon’ that both contact Mediator (Extended Data Fig. 5a). In the following, we will first describe the human Mediator structure and then discuss the Mediator–PIC interfaces and their implications for Mediator function.

Structure of human Mediator

The structure of human Mediator resembles that of yeast Mediator²³, and confirms the high conservation of Mediator structure across eukaryotic organisms^{29,30} (Fig. 2, Extended Data Fig. 5b, Supplementary Fig. 1). The head-module subunits MED6 and MED8 form the ‘neck’ region, and MED18, MED20 and the C-terminal helix of MED8 form the

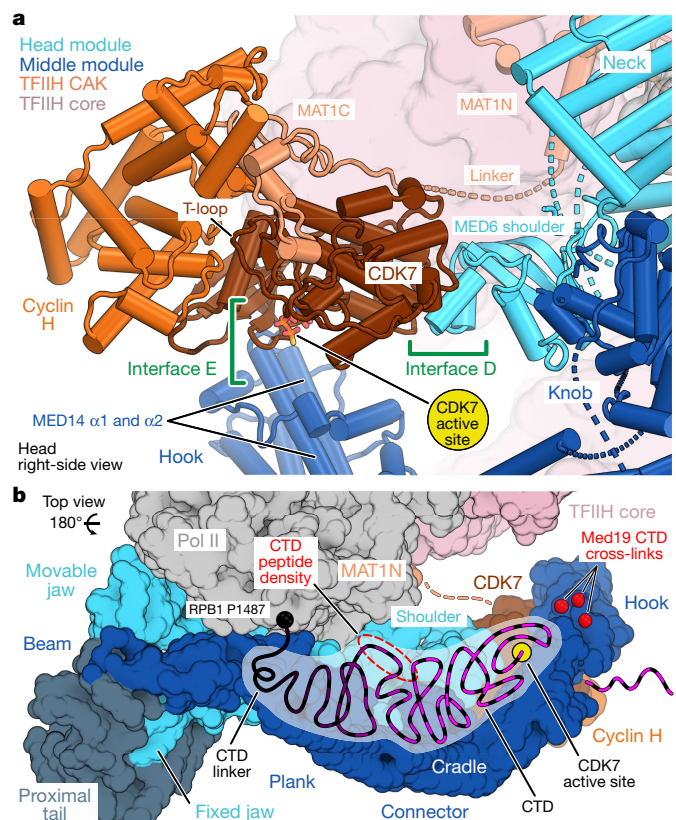


Fig. 4 | Interactions between Mediator and TFIH kinase. **a**, Interfaces D and E. The location of the CDK7 active site is highlighted by modelling of an ATP analogue²⁸. **b**, Putative path of the CTD from the CTD linker (black) through the cradle to the active site of CDK7 (yellow circle). Indicated are known sites of CTD cross-links⁹ and density for a CTD peptide bound to the Mediator head¹⁸, both obtained from the yeast system.

‘movable jaw’ (Fig. 2a). The head subunit MED17 shows some variations; its tooth domain is rotated and its nose domain is rotated and extended (Fig. 2b, c). Human Mediator also contains a helical insertion (residues 386–423) between its tooth and nose domains (Fig. 2d). The head subunits MED11 and MED22 contain longer C-terminal helices that protrude from the ‘fixed jaw’ (Fig. 2b, d). Compared with the yeast core Mediator in its PIC-bound state⁹, the middle module of the human Mediator is slightly rotated and shifted with respect to the head (Extended Data Fig. 5b). These movements are accommodated by tethering helices that are flexibly linked to subunits MED6 and MED17 and bind the middle module as observed before⁹. The ‘plank’ domain⁷ protrudes from the middle module and is mobile.

Our structure also reveals the proximal part of the tail module (‘proximal tail’), which is anchored on the head module and includes the newly observed subunits MED27–MED30 (Figs. 1, 2b). MED27 forms a RWD domain with a C-terminal zinc-finger motif and nestles in between the fixed and the movable jaws of the head module. MED27 also contacts MED20, the extended C-terminal region and nose domain of MED17, and a region in the MED14 beam. MED28 and MED30 contain long C-terminal helices that form a four-helix bundle with the C-terminal helices of MED11 and MED22. An N-terminal helix of MED28 is oriented at right angles to the C-terminal helix and is part of a second four-helix bundle that is poorly resolved owing to its peripheral location. Our structure of the PIC-bound human Mediator is generally consistent with cryo-EM studies of the mouse Mediator in an unbound state³¹. While our manuscript was under revision, the structure of the unbound mouse Mediator became available, which in addition contains subunits of the distal tail³².

Interfaces between Mediator and the core PIC

Our structure shows that the Mediator head module binds the core of the PIC by formation of the previously described^{7,9} interfaces A and B (Fig. 3). Interface A is formed by contacts of the MED18 subunit in the movable jaw with the TFIIB B-ribbon and the TFIIE E-ribbon (Fig. 3b). Interface B is formed by interactions of the neck submodule with the RPB4–RPB7 stalk of Pol II (Fig. 3c). In particular, the arm domain of MED8 and the spine domain of MED22 both contact the stalk subunit RPB4, including its C-terminal helix (Fig. 3c). Compared with its yeast counterpart, the neck submodule resides slightly closer to the Pol II stalk, resulting in a larger contact surface with the PIC. We do not observe the previously described^{7,9} interface C in our structure. However, movements in the middle module may occur and enable the formation of interface C by establishing a contact between the mobile plank of Mediator and the foot domain of Pol II, as described for the yeast Mediator–core PIC complex^{7,9}.

Mediator–TFIIH kinase interactions

Our structure also reveals the TFIIH module CAK, which is anchored to the PIC via its subunit MAT1 (Fig. 4). Whereas the N-terminal region of MAT1 binds the TFIIH core and the Pol II clamp, the C-terminal region (MAT1C) associates with the CDK7–cyclin H pair. The CDK7–cyclin H–MAT1C trimer is flexibly linked to the rest of the PIC²⁵, but in our structure it adopts a defined location that is similar to that in yeast Mediator–PIC complexes^{8,9}. In contrast to previous studies, we can, however, define the orientation of the CDK7–cyclin H–MAT1C trimer and its interactions with Mediator.

Mediator contacts the CAK module only through the CDK7 subunit and forms two distinct interfaces with CDK7 that we call interfaces D and E (Fig. 4a). Interface D is formed by contacts between the N-terminal region of the MED6 shoulder domain and two CDK7 surface regions (around residues 103–110 and 259–266) that differ in other kinases of the CDK family³³. Interface E is formed between the hook domain of the middle module—including the MED14 N-terminal region that comprises helices $\alpha 1$ and $\alpha 2$ —and the CDK7 N-terminal region (residues 10–26). This N-terminal region of CDK7 flanks the ATP-binding site and active centre. The corresponding N-terminal region of related enzymes is known to be involved in kinase activation³⁴. Whereas interface D is more extended and may hold the CDK7–cyclin H–MAT1C trimer in position, interface E is likely to be transient because the Mediator hook is mobile. Consistent with the observed CAK–Mediator contacts, the activity of the PIC in phosphorylating Ser5 residues in the C-terminal domain (CTD) was stimulated around 4.5-fold by the addition of recombinant Mediator (Extended Data Fig. 1c).

These observations have implications for our understanding of how Mediator stimulates CDK7-dependent phosphorylation of the Pol II CTD. First, Mediator holds the flexibly linked CDK7–cyclin H–MAT1C trimer in a defined position. Second, Mediator orients the trimer such that the active site of CDK7 faces the previously described cradle⁷, an open space that is formed between Mediator and the PIC. The orientation of CDK7 may facilitate targeting of the CTD substrate to the kinase, as the CTD may extend from the Pol II linker through the cradle to reach the CDK7 active site (Fig. 4b). This path is generally consistent with cross-linking sites⁹ and with density for a CTD peptide¹⁸ that were both obtained with the yeast system. Third, the Mediator hook may stimulate kinase activity by allosterically inducing an active conformation of the CDK7 catalytic centre, maybe cooperating with the T-loop of CDK7^{28,35}.

Conclusions

Together with the accompanying paper²⁵, our work provides the structural basis for understanding how transcription initiation is

regulated at eukaryotic genes. Comparison with the structure of the yeast Mediator–PIC highlights the high conservation of the transcription initiation machinery throughout eukaryotes. Work can now focus on different functional states of the Mediator–PIC complex and the influence of activators. In addition, our recombinant human Mediator will enable analysis of gene-regulatory mechanisms by site-directed mutagenesis. During the revision of our manuscript, an independently derived structure of the human Mediator–PIC complex became available³⁶; this structure also shows the distal tail of Mediator and two short CTD regions, suggesting that the tail stabilizes Mediator–CTD interactions.

Online content

Any methods, additional references, Nature Research reporting summaries, source data, extended data, supplementary information, acknowledgements, peer review information; details of author contributions and competing interests; and statements of data and code availability are available at <https://doi.org/10.1038/s41586-021-03555-7>.

- Malik, S. & Roeder, R. G. Transcriptional regulation through Mediator-like coactivators in yeast and metazoan cells. *Trends Biochem. Sci.* **25**, 277–283 (2000).
- Kornberg, R. D. Mediator and the mechanism of transcriptional activation. *Trends Biochem. Sci.* **30**, 235–239 (2005).
- Schier, A. C. & Taatjes, D. J. Structure and mechanism of the RNA polymerase II transcription machinery. *Genes Dev.* **34**, 465–488 (2020).
- Kim, Y. J., Björklund, S., Li, Y., Sayre, M. H. & Kornberg, R. D. A multiprotein mediator of transcriptional activation and its interaction with the C-terminal repeat domain of RNA polymerase II. *Cell* **77**, 599–608 (1994).
- Malik, S. & Roeder, R. G. The metazoan Mediator co-activator complex as an integrative hub for transcriptional regulation. *Nat. Rev. Genet.* **11**, 761–772 (2010).
- Conaway, R. C. & Conaway, J. W. Origins and activity of the Mediator complex. *Semin. Cell Dev. Biol.* **22**, 729–734 (2011).
- Plaschka, C. et al. Architecture of the RNA polymerase II–Mediator core initiation complex. *Nature* **518**, 376–380 (2015).
- Robinson, P. J. et al. Structure of a complete Mediator–RNA polymerase II pre-initiation complex. *Cell* **166**, 1411–1422 (2016).
- Schilbach, S. et al. Structures of transcription pre-initiation complex with TFIIH and Mediator. *Nature* **551**, 204–209 (2017).
- Elmlund, H. et al. The cyclin-dependent kinase 8 module sterically blocks Mediator interactions with RNA polymerase II. *Proc. Natl Acad. Sci. USA* **103**, 15788–15793 (2006).
- Tsai, K. L. et al. A conserved Mediator–CDK8 kinase module association regulates Mediator–RNA polymerase II interaction. *Nat. Struct. Mol. Biol.* **20**, 611–619 (2013).
- Knuesel, M. T., Meyer, K. D., Bernecky, C. & Taatjes, D. J. The human CDK8 subcomplex is a molecular switch that controls Mediator coactivator function. *Genes Dev.* **23**, 439–451 (2009).
- Chadick, J. Z. & Asturias, F. J. Structure of eukaryotic Mediator complexes. *Trends Biochem. Sci.* **30**, 264–271 (2005).
- Larivière, L., Seizl, M. & Cramer, P. A structural perspective on Mediator function. *Curr. Opin. Cell Biol.* **24**, 305–313 (2012).
- Plaschka, C., Nozawa, K. & Cramer, P. Mediator architecture and RNA polymerase II interaction. *J. Mol. Biol.* **428**, 2569–2574 (2016).
- Imasaki, T. et al. Architecture of the Mediator head module. *Nature* **475**, 240–243 (2011).
- Larivière, L. et al. Structure of the Mediator head module. *Nature* **492**, 448–451 (2012).
- Robinson, P. J., Bushnell, D. A., Trnka, M. J., Burlingame, A. L. & Kornberg, R. D. Structure of the Mediator Head module bound to the carboxy-terminal domain of RNA polymerase II. *Proc. Natl Acad. Sci. USA* **109**, 17931–17935 (2012).
- Wang, X. et al. Redefining the modular organization of the core Mediator complex. *Cell Res.* **24**, 796–808 (2014).
- Tsai, K. L. et al. Subunit architecture and functional modular rearrangements of the transcriptional mediator complex. *Cell* **157**, 1430–1444 (2014).
- Tsai, K. L. et al. Mediator structure and rearrangements required for holoenzyme formation. *Nature* **544**, 196–201 (2017).
- Cevher, M. A. et al. Reconstitution of active human core Mediator complex reveals a critical role of the MED14 subunit. *Nat. Struct. Mol. Biol.* **21**, 1028–1034 (2014).
- Nozawa, K., Schneider, T. R. & Cramer, P. Core Mediator structure at 3.4 Å extends model of transcription initiation complex. *Nature* **545**, 248–251 (2017).
- Egley, J. M. & Cohn, F. A history of TFIIH: two decades of molecular biology on a pivotal transcription/repair factor. *DNA Repair* **10**, 714–721 (2011).
- Aibara, S., Schilbach, S. & Cramer, P. Structures of mammalian RNA polymerase II pre-initiation complexes. *Nature* <https://doi.org/10.1038/s41586-021-03554-8> (2021).
- Kocic, G. et al. Structural basis of TFIIH activation for nucleotide excision repair. *Nat. Commun.* **10**, 2885 (2019).
- Vos, S. M., Farnung, L., Urlaub, H. & Cramer, P. Structure of paused transcription complex Pol II–DSIF–NELF. *Nature* **560**, 601–606 (2018).
- Greber, B. J. et al. The cryoelectron microscopy structure of the human CDK-activating kinase. *Proc. Natl Acad. Sci. USA* **117**, 22849–22857 (2020).

29. Asturias, F. J., Jiang, Y. W., Myers, L. C., Gustafsson, C. M. & Kornberg, R. D. Conserved structures of Mediator and RNA polymerase II holoenzyme. *Science* **283**, 985–987 (1999).
30. Bourbon, H. M. et al. A unified nomenclature for protein subunits of Mediator complexes linking transcriptional regulators to RNA polymerase II. *Mol. Cell* **14**, 553–557 (2004).
31. El Khattabi, L. et al. A pliable Mediator acts as a functional rather than an architectural bridge between promoters and enhancers. *Cell* **178**, 1145–1158 (2019).
32. Zhao, H. et al. Structure of mammalian Mediator complex reveals Tail module architecture and interaction with a conserved core. *Nat. Commun.* **12**, 1355 (2021).
33. Lolli, G., Lowe, E. D., Brown, N. R. & Johnson, L. N. The crystal structure of human CDK7 and its protein recognition properties. *Structure* **12**, 2067–2079 (2004).
34. Wood, D. J. & Endicott, J. A. Structural insights into the functional diversity of the CDK-cyclin family. *Open Biol.* **8**, 180112 (2018).
35. Peissert, S., Schlosser, A., Kendel, R., Kuper, J. & Kisker, C. Structural basis for CDK7 activation by MAT1 and cyclin H. *Proc. Natl Acad. Sci. USA* **117**, 26739–26748 (2020).
36. Abdella, R. et al. Structure of the human Mediator-bound transcription preinitiation complex. *Science* **372**, 52–56 (2021).
37. Cramer, P., Bushnell, D. A. & Kornberg, R. D. Structural basis of transcription: RNA polymerase II at 2.8 Å resolution. *Science* **292**, 1863–1876 (2001).

Publisher's note Springer Nature remains neutral with regard to jurisdictional claims in published maps and institutional affiliations.

© The Author(s), under exclusive licence to Springer Nature Limited 2021

Methods

Data reporting

No statistical methods were used to predetermine sample size. The experiments were not randomized and the investigators were not blinded to allocation during experiments and outcome assessment.

Cloning and protein expression

Full length cDNA clones of 20 human Mediator subunits were either obtained from the Harvard Plasmid Repository or chemically synthesized by Integrated DNA Technologies (IDT). cDNAs were used as PCR templates for cloning into modified pFastBac vectors (derivatives of 438-A and 438-C; Addgene 55218 and 55220) by ligation-independent cloning (LIC)³⁸. All subunits were cloned without an affinity tag, except for an N-terminal 6×His– maltose-binding protein (MBP) tag, followed by a tobacco etch virus (TEV) protease site on MED17 and a N-terminal MBP-tag on MED14 with a cleavable TEV protease site. Three different constructs for baculovirus expression were generated, one containing the seven subunits of the head module (MED6, MED8, MED11, MED17, MED18, MED20 and MED22), one for head-associated²⁰ metazoan-specific subunits (MED26, MED27, MED28, MED29 and MED30) and one for the middle-module subunits (MED4, MED7, MED9, MED10, MED14, MED19, MED21 and MED31). We refer to these three constructs as C1, C2 and C3, respectively. Whereas C1 and C2 were generated by a biGBC cloning methodology³⁹, C3 was made using multiple rounds of LIC³⁸. Final clones were verified by sequencing. Bacmid preparation and virus production (V0 and V1 stages in *Spodoptera frugiperda* Sf9 cells and Sf21 cells, respectively) were performed as described⁴⁰. Expression of Mediator in insect cells was achieved by co-infection of the V1 virus for the constructs C1, C2 and C3 in Hi5 cells (Expression Systems). After 60 h of expression, cells were collected by centrifugation (900g, 10 min, 4 °C) and resuspended in buffer-A (25 mM 4-(2-hydroxyethyl)-1-piperazineethanesulfonic acid (HEPES) pH 7.5, 300 mM NaCl, 10% glycerol (v/v), 0.5 mM Tris(2-carboxyethyl) phosphine (TCEP), 0.284 µg/ml leupeptin, 1.37 µg/ml pepstatin A, 0.17 mg/ml PMSF and 0.33 mg/ml benzamide). The cell suspension was flash-frozen in liquid nitrogen and stored at –80 °C.

Protein purification

All steps of protein purification were performed at 4 °C. Recombinant Mediator was purified by successive steps of affinity chromatography followed by ion-exchange chromatography and size-exclusion chromatography (SEC). Stored insect cell suspension was thawed at 25 °C. Cells were lysed by sonication and clarified by centrifugation (79,000g, 60 min). The supernatant was passed over amylose resin (New England Biolabs) packed in an Econo-column (Bio-Rad) pre-equilibrated with buffer-A and then washed with 20 column volumes (CV) of buffer-A. cMED was eluted with buffer-B (25 mM HEPES pH 7.5, 100 mM NaCl, 10% glycerol (v/v) and 0.5 mM TCEP) containing 100 mM maltose and incubated overnight with TEV protease. The cleaved MBP tag and TEV protease were removed by anion-exchange chromatography using a Mono Q5/50GL column (GE Healthcare) pre-equilibrated with buffer-B. After sample application, the column was washed with 5 CV of buffer-B and proteins were eluted with a linear gradient from 0–100% of buffer-C (25 mM HEPES pH 7.5, 1M NaCl, 10% glycerol (v/v) and 0.5 mM TCEP) in 40 CV. Fractions containing recombinant Mediator were pooled, concentrated using a 100-kDa MWCO Amicon Ultra Centrifugal Filter (Merck) and injected onto a Superose 6 increase 10/300 GL column (GE Healthcare) pre-equilibrated with buffer-A. Fractions were analysed by SDS–PAGE and the homogenous peak fractions were pooled and concentrated to 4.5 mg/ml using a 100-kDa MWCO Amicon Ultra Centrifugal Filter (Merck). Concentrated Mediator was aliquoted, flash-frozen in liquid nitrogen and stored at –80 °C until use. Pol II, TBP, TFIIA, TFIIB, TFIIE and TFIIF were purified as previously described²⁵ and the TFIIH core and the TFIIH kinase module (CAK) were purified as previously described²⁶.

Preparation of the human Mediator–PIC complex

We formed a Mediator–PIC complex with promoter DNA at 25 °C following our previously reported assembly method⁷. We used a 106-base-pair adenoviral major late promoter (AdMLP) DNA duplex (template: 5'-AGGGAGTACTCACCCCAACAGCTGGCCCTCGCAGACGCGATGCGGAA GAGAGTGAGGACGGAACGCGCCCCACCCCTTTTATAGCCCCCTTC AGGAACACCCG-3'; non-template: 5'-CGGGTGTCTCTGAAGGGGGCT ATAAAAGGGGGTGGGGGCGCGTTCGTCCTCACTCTCTCCGCATCGCT GTCTGCGAGGGCCAGCTGTT GGGGTGAGTACTCCCT-3'). In brief, the 10-subunit TFIIH was obtained by pre-incubating the TFIIH core with the TFIIH CAK. Then, TBP–TFIIA–TFIIB was pre-bound to the AdMLP scaffold to form the upstream complex and mixed with a pre-formed Pol II–TFIIF complex. After this, TFIIE and TFIIF were added in 2-min intervals to form the PIC. Finally, Mediator was added to form the Mediator–PIC complex and this step was supplemented with ADP–BeF₃. The mixture was incubated at 25 °C for 120 min at 400 r.p.m. and aggregates were removed by centrifugation at 21,000g for 5 min. The reconstituted Mediator–PIC complex was subjected to sucrose-gradient centrifugation in a 4-ml centrifugation tube (Beckmann Coulter) with simultaneous cross-linking⁴¹. The gradient was prepared using a BioComp Gradient Master 108 (BioComp Instruments) by mixing a 15% sucrose solution (15% sucrose, 25 mM HEPES pH 7.6, 100 mM KCl, 5 mM MgCl₂, 5% glycerol (v/v) and 3 mM TCEP) and a 40% sucrose solution (40% sucrose, 25 mM HEPES pH 7.6, 100 mM KCl, 5 mM MgCl₂, 5% glycerol (v/v) and 3 mM TCEP) supplemented with 0.25% of glutaraldehyde (v/v) cross-linker. The sample was centrifuged at 175,000g for 16 h at 4 °C. Fractions of 200 µl were collected manually and the cross-linking reaction was quenched with a cocktail of 10 mM aspartate and 30 mM lysine for 10 min. Fractions containing the Mediator–PIC complex were dialysed against buffer-D (25 mM HEPES pH 7.6, 100 mM KCl, 5 mM MgCl₂, 5% glycerol and 3 mM TCEP) to remove sucrose.

Cryo-EM data collection and processing

To prepare grids for cryo-EM, Quantifoil R3.5/1 holey carbon grids were pre-coated with an amorphous carbon and glow-discharged for 45 s. Four microlitres of Mediator–PIC sample was added to the carbon top and incubated for 5 min. The grids were blotted for 2.5 s and vitrified by plunging into liquid ethane with a Vitrobot Mark IV (FEI Company) set at 4 °C and 100% humidity. Cryo-EM data were collected on the 300-kV FEI Titan Krios with a K3 summit direct detector (Gatan) and a GIF quantum energy filter (Gatan) operated with a slit width of 20 eV. Automated data collection was performed with SerialEM at a nominal magnification of 81,000×, corresponding to a pixel size of 1.05 Å/pixel⁴². A total of 21,894 image stacks, with each stack containing 40 frames, were collected at a defocus range of –0.3 to –5.0 µm. All movie frames were contrast transfer function (CTF)-estimated, motion-corrected and dose-weighted using Warp⁴³. Particles were picked by Warp using the trained neural network instance BoxNet, resulting in 2,309,888 particles as a starting set. Subsequent steps of image processing were performed with cryoSPARC⁴⁴ and RELION v.3.1.0⁴⁵.

Particles were extracted with a binning factor of 4 and a box size of 120 pixels (a pixel size of 4.2 Å/pixel) to perform initial clean-up and sorting. The first major focus of processing was to identify the best Mediator-containing classes. By performing multiple rounds of heterogenous and homogenous refinements in cryoSPARC⁴⁴, a set of 294,904 particles (Set-1) containing Mediator–PIC was identified. Set-1 was re-extracted without binning and processed with RELION v.3.1.0, as follows. The particles were first refined using a 3D refinement followed by a focused 3D classification with a large spherical mask (Mask-1) encompassing the region of Mediator and the Pol II stalk. This resulted in identifying the best 85,182 Mediator-containing particles (Set-2). These particles were again subjected to focused 3D refinement using Mask-1, giving rise to a Mediator–Pol II stalk reconstruction at 4.0 Å resolution. In parallel, focused 3D classification of Set1 with a spherical

mask (Mask-2) around the TFIID-exit DNA region helped to identify the best 83,713 TFIID-containing particles (Set-3). Particles from Set-3 were then subjected to focused 3D refinement with Mask-2 to arrive at a 6.5 Å map of TFIID (Map-2). Finally, the best Mediator–PIC-containing 25,967 particles (Set-4) were identified by finding particles present in both Set-2 and Set-3. A consensus 3D refinement of Set-4 led to a final reconstruction of the entire Mediator–PIC ensemble at 4.5 Å resolution. The reported resolutions were calculated on the basis of the gold standard Fourier shell correlation (FSC) 0.143 criterion. After processing of the final reconstructions of Mediator–Pol II stalk, TFIID and Mediator–PIC *B*-factor sharpening was performed for all three final maps on the basis of automatic *B*-factor determination in RELION (−85 Å² for Mediator–Pol II stalk, 0 Å² for TFIID and −80 Å² for PIC–Mediator). Estimates of local resolution were calculated using the in-built local-resolution tool of RELION and the estimated *B*-factors. To assist model building, a local-resolution-filtered map (but unsharpened) of Mediator–Pol II stalk was sharpened locally using PHENIX.auto_sharpen.

Model building and refinement

The PIC was modelled using its high-resolution structure in the closed promoter state, which contains the ATPase subunit XPB in the nucleotide-free pre-translocation conformation²⁵. The presence of ADP–BeF₃ in our Mediator–PIC preparation is expected to lead to the post-translocated conformation of XPB. However, the local resolution did not allow us to unambiguously detect the XPB conformation. We therefore did not alter XPB in the PIC structure that was used.

Homology models of all 15 core Mediator subunits were generated by SWISS-Model⁴⁶ using the high-resolution structures of the yeast Mediator²³. The seven subunits of the head module and the middle module subunits MED14 and MED31 were initially built by placing the homology models into the density using rigid-body fitting in Chimera⁴⁷. The divergent parts of these subunits were manually adjusted in Coot⁴⁸ to fit the density. The metazoan specific subunits MED27–MED30 of the proximal tail were manually built de novo using Coot. The helices and strands of all subunits were placed and built with confidence in their register using bulky residues as sequence markers. Ambiguous densities of loops connecting the helices and strands were not modelled. The resulting model of the Mediator bound to the Pol II stalk was real-space-refined in PHENIX⁴⁹ and subjected to multiple rounds of manual adjustment and real-space refinement in Coot and PHENIX, respectively, to achieve the final model with good stereochemistry as assessed by MolProbity⁵⁰.

The Mediator middle module was built on the basis of the published yeast structure²³ as follows. A conservative homology model of the middle module lacking the MED14 beam was generated from the homology models of the single Mediator subunits and placed into the Mediator–Pol II stalk focused-refined cryo-EM map low-pass-filtered to 12 Å in Coot⁴⁸. The model was stripped of flexible loops and long-chain termini. We manually adjusted the trajectories of the helices in the connector and hook regions and in proximity to the knob, and parts of MED4, MED7 and MED14 that were interacting with MED31. The model was adapted to the cryo-EM density of the Mediator–PIC cryo-EM map by flexible fitting with NAMDinator⁵¹, and was corrected for geometry outliers in alternating rounds of manual adjustment in Coot⁴⁸ and real-space refinement in PHENIX⁴⁹.

The final model was obtained by manually merging the resulting Mediator–Pol II stalk model with the atomic model of the PIC²⁵ lacking the Pol II stalk. The Mediator–PIC model was first manually examined against the Mediator–PIC overall map in Coot and then real-space refinement was performed with PHENIX. The final model showed good stereochemistry as assessed by MolProbity⁵⁰ (Extended Data Table 1). Figures representing the structures and maps were prepared using PyMOL and UCSF ChimeraX.

Pol II CTD phosphorylation assay

Reconstituted PIC or Mediator–PIC was incubated with 3 mM ATP for 15 s at 4 °C and the reaction was stopped by adding 4× LDS loading

buffer (Invitrogen). The samples were run on 4–12% SDS–PAGE in MOPS buffer (Thermo Fisher Scientific) and transferred to a PVDF membrane (GE Healthcare Life Sciences). The membrane was blocked with 5% (w/v) milk powder in 1% PBS containing 0.1% Tween 20 (1× PBST) for 1 h at room temperature. The membranes were then cut into half and incubated overnight at 4 °C with antibodies against Ser5 (3E8) (1:2,000 dilution, Sigma-Aldrich) or against RPB3 (1:2,000, Bethyl Laboratories) diluted in 2% milk powder containing PBST. Membranes were washed three times with PBST. Horseradish peroxidase (HRP)-conjugated anti-rat secondary antibody (1:5,000) (Sigma-Aldrich A9037) was incubated with the membrane portion treated for 1 h at room temperature with Ser5 antibody, whereas the membrane portion containing RPB3 was treated with HRP-conjugated anti-rabbit (1:5,000) (GE Healthcare Life Sciences) in 1% milk powder containing PBST. SuperSignal West Pico Chemiluminescent Substrate (Thermo Fisher Scientific) was used for detection of proteins. Membranes were imaged with an Advanced Fluorescent Imager (Intas) and western blot signals were quantified with ImageJ. Phosphorylation experiments were performed in triplicate. Mean and standard deviation values were calculated and signals were normalized to the mean of the PIC samples. The statistical significance of the results was determined using a one-tailed unpaired *t*-test assuming equal variances.

Structure-based sequence alignment

Structure-based sequence alignment comparing the respective Mediator subunits from humans and *Schizosaccharomyces pombe* was performed using the Expresso algorithm of the T-Coffee server⁵². The alignments were manually corrected for discrepancies and the secondary structure labels were assigned using the program ESPript from the ENDscript server⁵³.

Reporting summary

Further information on research design is available in the Nature Research Reporting Summary linked to this paper.

Data availability

The cryo-EM density reconstructions and models were deposited with the Electron Microscopy Data Bank (EMDB) (accession codes EMD-12609 for Mediator in complex with the Pol II stalk and EMD-12610 for Mediator in complex with the PIC) and with the Protein Data Bank (PDB) (accession code 7NVR). All data are available in the Article or its supplementary files. Source data are provided with this paper.

38. Gradia, S. D. et al. MacroBac: new technologies for robust and efficient large-scale production of recombinant multiprotein complexes. *Methods Enzymol.* **592**, 1–26 (2017).
39. Weissmann, F. et al. biGBac enables rapid gene assembly for the expression of large multisubunit protein complexes. *Proc. Natl Acad. Sci. USA* **113**, E2564–E2569 (2016).
40. Farnung, L., Vos, S. M., Wigge, C. & Cramer, P. Nucleosome–Chd1 structure and implications for chromatin remodelling. *Nature* **550**, 539–542 (2017).
41. Kastner, B. et al. GraFix: sample preparation for single-particle electron cryomicroscopy. *Nat. Methods* **5**, 53–55 (2008).
42. Mastrorade, D. N. Automated electron microscope tomography using robust prediction of specimen movements. *J. Struct. Biol.* **152**, 36–51 (2005).
43. Tegunov, D. & Cramer, P. Real-time cryo-electron microscopy data preprocessing with Warp. *Nat. Methods* **16**, 1146–1152 (2019).
44. Punjani, A., Rubinstein, J. L., Fleet, D. J. & Brubaker, M. A. cryoSPARC: algorithms for rapid unsupervised cryo-EM structure determination. *Nat. Methods* **14**, 290–296 (2017).
45. Zivanov, J. et al. New tools for automated high-resolution cryo-EM structure determination in RELION-3. *eLife* **7**, e42166 (2018).
46. Waterhouse, A. et al. SWISS-MODEL: homology modelling of protein structures and complexes. *Nucleic Acids Res.* **46**, W296–W303 (2018).
47. Pettersen, E. F. et al. UCSF Chimera—a visualization system for exploratory research and analysis. *J. Comput. Chem.* **25**, 1605–1612 (2004).
48. Casañal, A., Lohkamp, B. & Emsley, P. Current developments in Coot for macromolecular model building of electron cryo-microscopy and crystallographic data. *Protein Sci.* **29**, 1055–1064 (2020).
49. Liebschner, D. et al. Macromolecular structure determination using X-rays, neutrons and electrons: recent developments in Phenix. *Acta Crystallogr. D* **75**, 861–877 (2019).
50. Prisant, M. G., Williams, C. J., Chen, V. B., Richardson, J. S. & Richardson, D. C. New tools in MolProbity validation: CaBLAM for cryoEM backbone, UnDowser to rethink “waters,” and NGL Viewer to recapture online 3D graphics. *Protein Sci.* **29**, 315–329 (2020).

Article

51. Kidmose, R. T. et al. Namdinator—automatic molecular dynamics flexible fitting of structural models into cryo-EM and crystallography experimental maps. *IUCr J* **6**, 526–531 (2019).
52. Notredame, C., Higgins, D. G. & Heringa, J. T-Coffee: a novel method for fast and accurate multiple sequence alignment. *J. Mol. Biol.* **302**, 205–217 (2000).
53. Robert, X. & Gouet, P. Deciphering key features in protein structures with the new ENDscript server. *Nucleic Acids Res.* **42**, W320–W324 (2014).

Acknowledgements We thank past and present members of the P.C. laboratory, particularly U. Neef, P. Rus and F. Grabbe for maintenance of the insect cell culture and purification of the recombinant human initiation factors; and we thank C. Dienemann and U. Steuerwald for maintenance of the cryo-EM facility. S.R. was supported by a Peter-and-Traudl-Engelhorn postdoctoral fellowship; S.A. was supported by an H2020 Marie Curie Individual Fellowship (894862); and P.C. was supported by the Deutsche Forschungsgemeinschaft (EXC 2067/1 39072994, SFB860 and SPP2191) and the ERC Advanced Investigator Grant CHROMATRANS (grant agreement no. 882357).

Author contributions S.R. performed all experiments and data analysis, except for the following: S.S. established the human PIC preparation; S.A. provided human PIC coordinates; S.A. and S.S. assisted with data processing and structural modelling; and C.D. assisted with cryo-EM grid preparation and data collection. P.C. designed and supervised research. S.R., S.S., S.A. and P.C. interpreted the data and wrote the manuscript.

Competing interests The authors declare no competing interests.

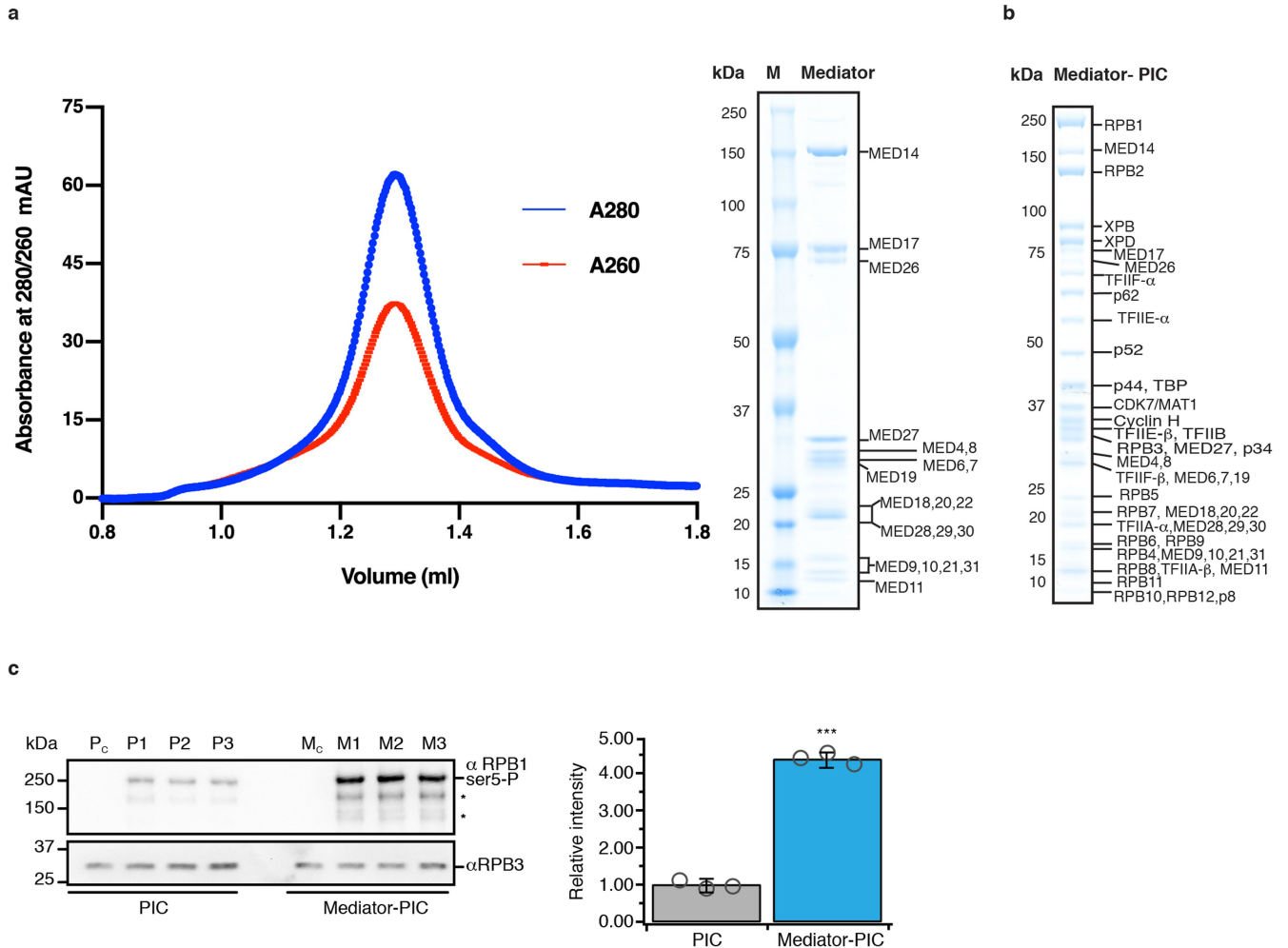
Additional information

Supplementary information The online version contains supplementary material available at <https://doi.org/10.1038/s41586-021-03555-7>.

Correspondence and requests for materials should be addressed to P.C.

Peer review information *Nature* thanks Steve Hahn and the other, anonymous, reviewer(s) for their contribution to the peer review of this work. Peer reviewer reports are available.

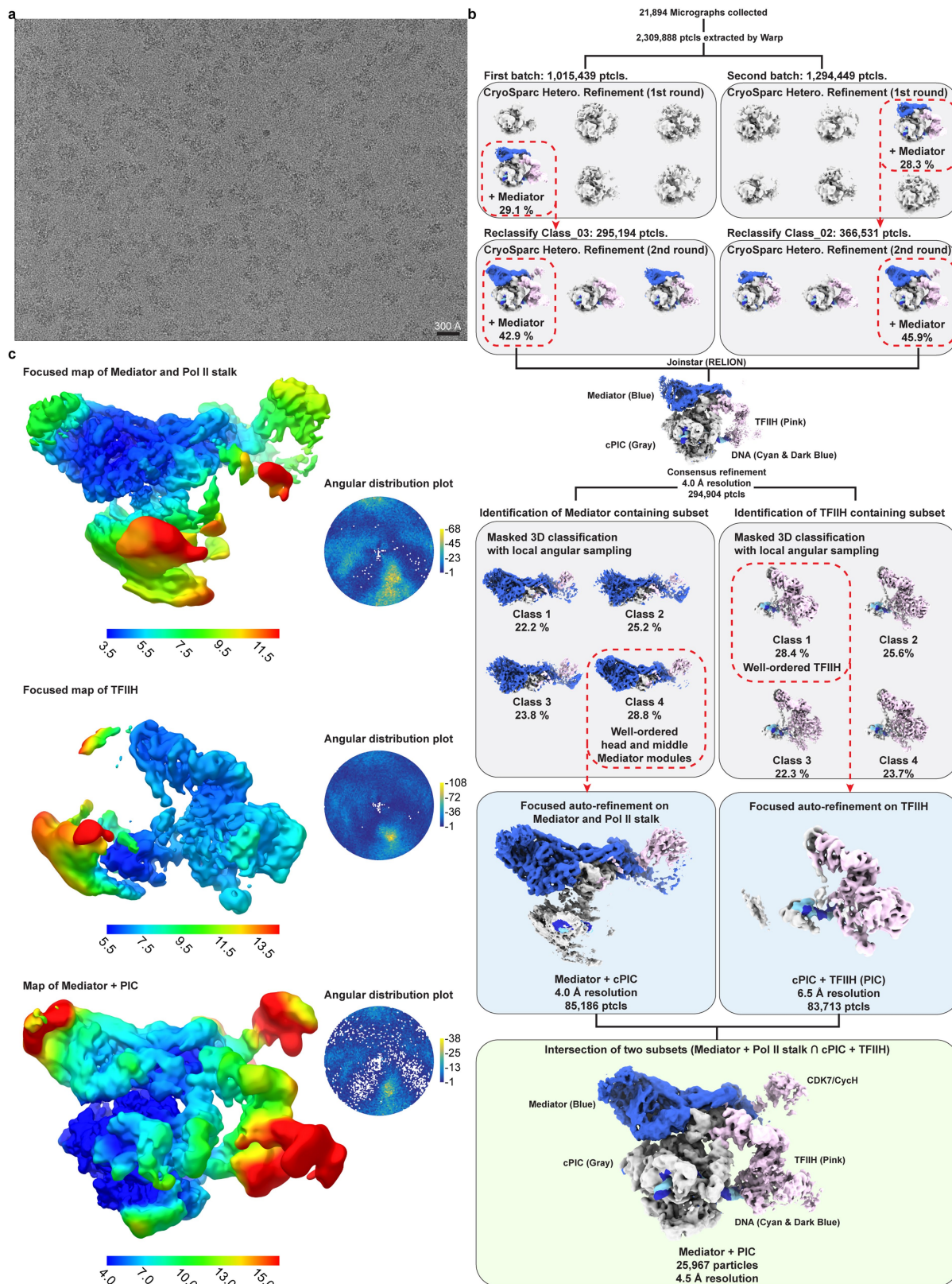
Reprints and permissions information is available at <http://www.nature.com/reprints>.



Extended Data Fig. 1 | Preparation of the human Mediator-PIC complex.

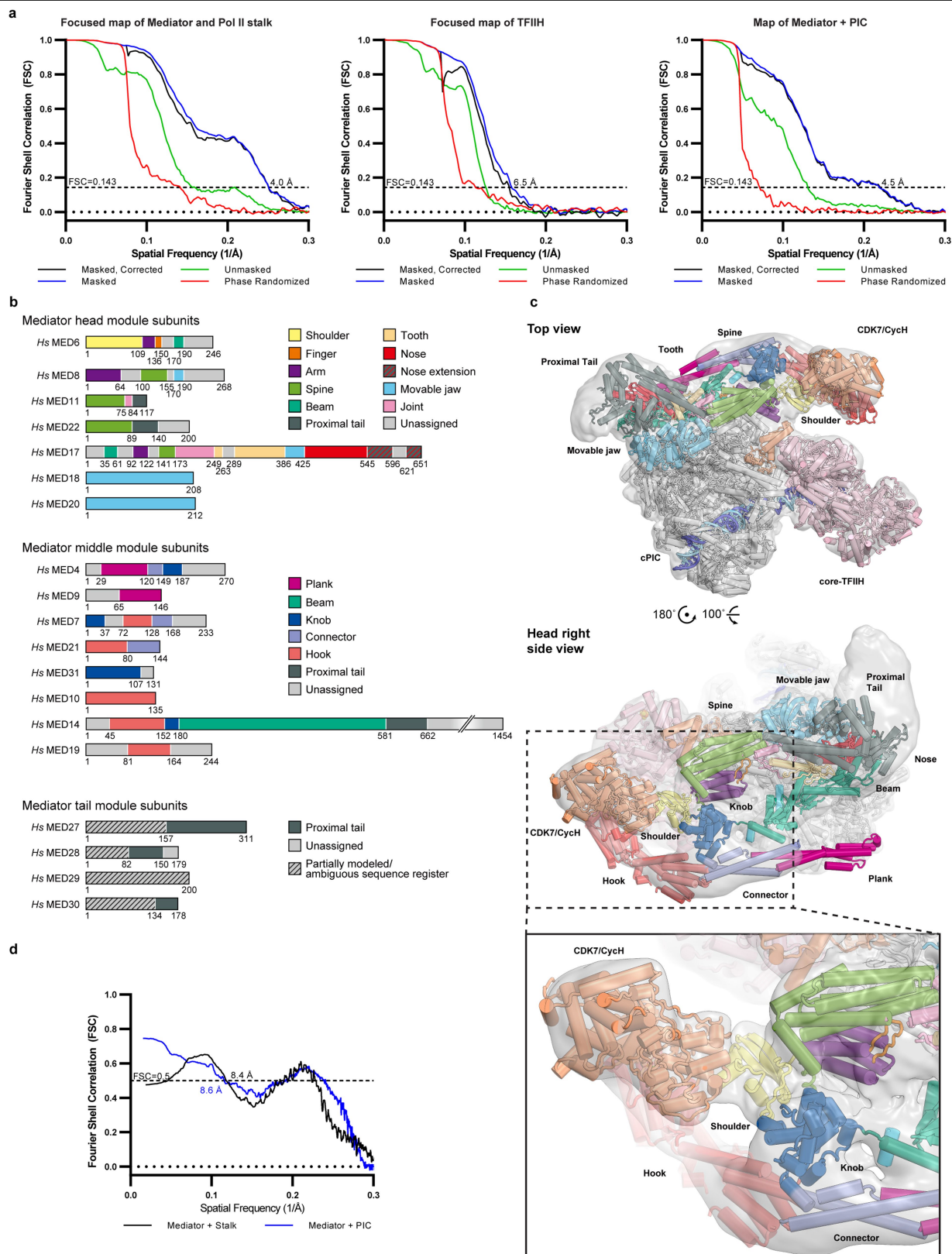
a, Size-exclusion chromatography of recombinant human Mediator shows a single peak. SDS-PAGE analysis (replicated three times) shows the presence of 20 Mediator subunits, confirmed by mass spectrometry (not shown). Raw SDS-PAGE data are provided in Supplementary Fig. 2. **b**, SDS-PAGE analysis of the human Mediator-PIC complex after isolation from a sucrose gradient (replicated three times). Raw SDS-PAGE data are provided in Supplementary Fig. 2. **c**, Recombinant 20-subunit human Mediator is able to stimulate Pol II CTD phosphorylation by CDK7 in the presence of ATP. Pol II CTD phosphorylation was assessed by western blotting against phosphorylated Ser5 of the CTD heptad repeat. An antibody against RPB3 was used to obtain

the loading control. Experiments were performed in triplicate (P1-P3 and M1-M3) and a negative control sample without ATP (P_c and M_c) was included to exclude prior CTD phosphorylation. The bar diagram illustrates an around 4.5-fold stimulation of Pol II CTD phosphorylation in the Mediator-PIC samples over the PIC samples. Data are mean ± s.d. of three independent experiments (replicated three times). The mean value of the triplicates was used as the centre measure for error bars (mean = 4.47). Statistical significance with a *P* value of 3.43×10^{-6} was determined using a one-tailed unpaired *t*-test (***P* < 0.001, ***P* < 0.01, **P* < 0.05). Raw data for the western blots are available in Supplementary Fig. 2.



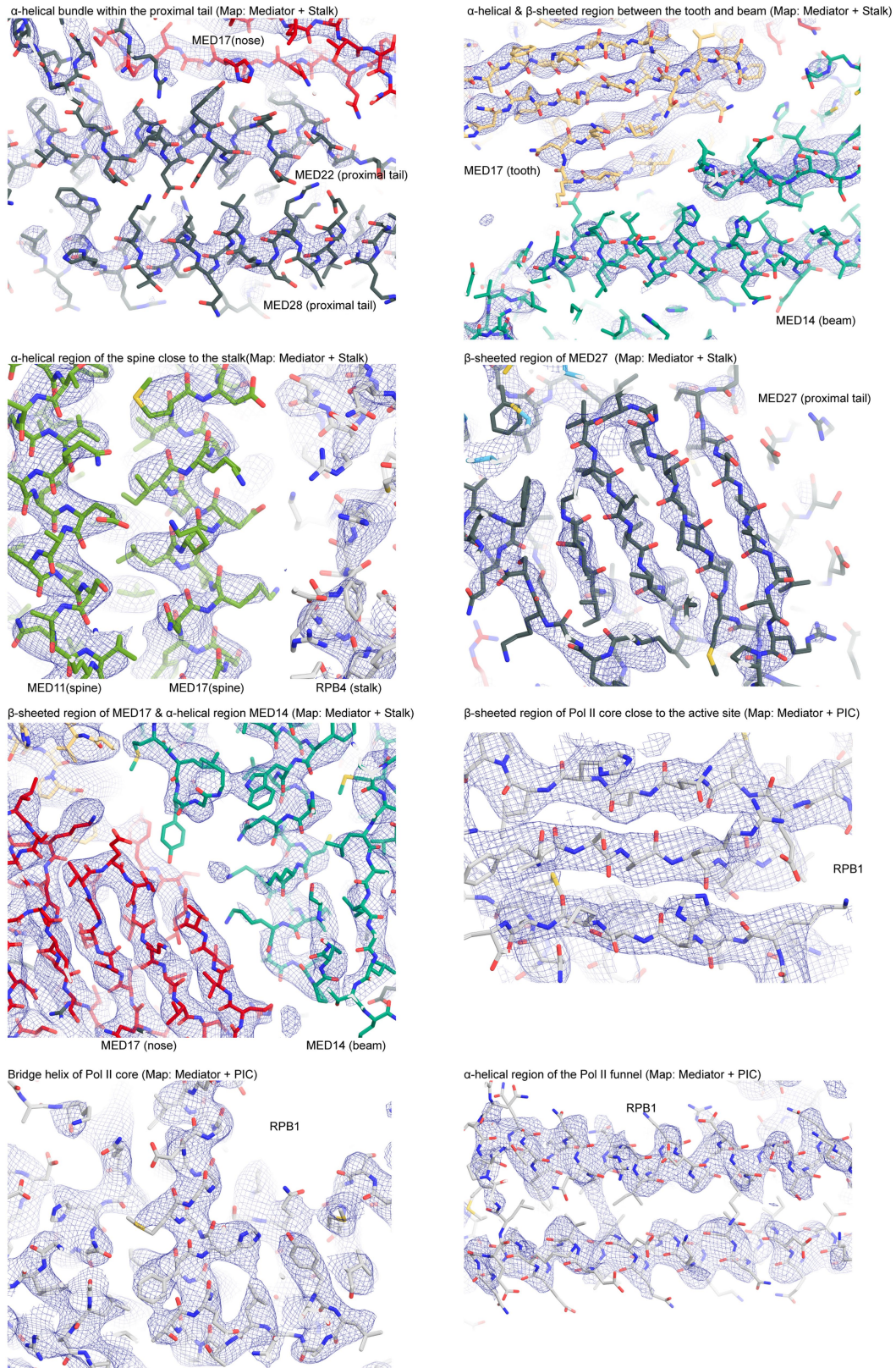
Extended Data Fig. 2 | Cryo-EM data processing. **a**, Representative cryo-EM micrograph of the human Mediator-PIC complex (replicated more than 20,000 times). Scale bar, 300 Å. **b**, Processing tree describing particle classification. Reconstructions that gave rise to maps used for model building are indicated (blue for focused maps, green for overall maps). Regions

corresponding to the core PIC (cPIC), TFIH (including the CAK), DNA, and Mediator are coloured in grey, pink, dark blue and cyan, and blue, respectively. **c**, Reconstructions coloured by their local resolution as estimated using RELION. In the angular distribution plots, colour indicates particle representation (white areas indicate unpopulated angles).

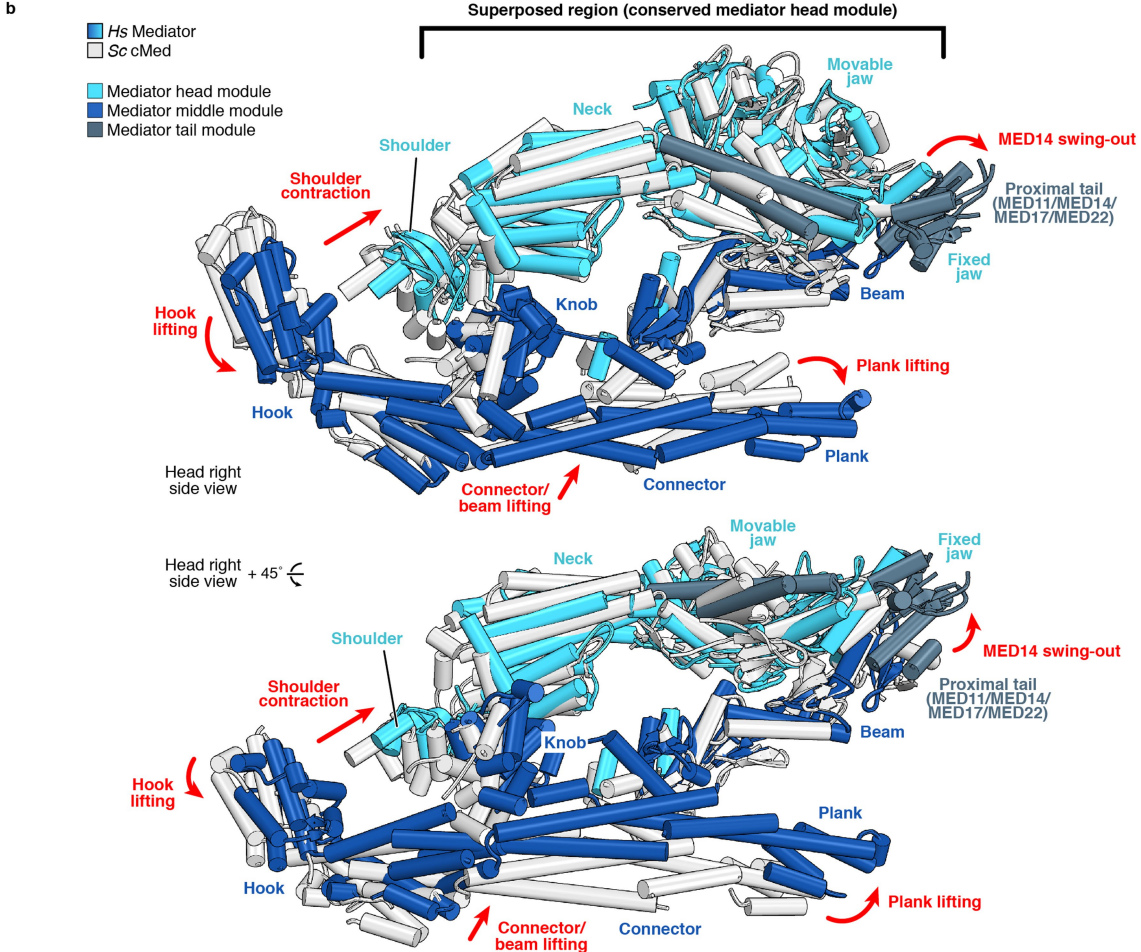
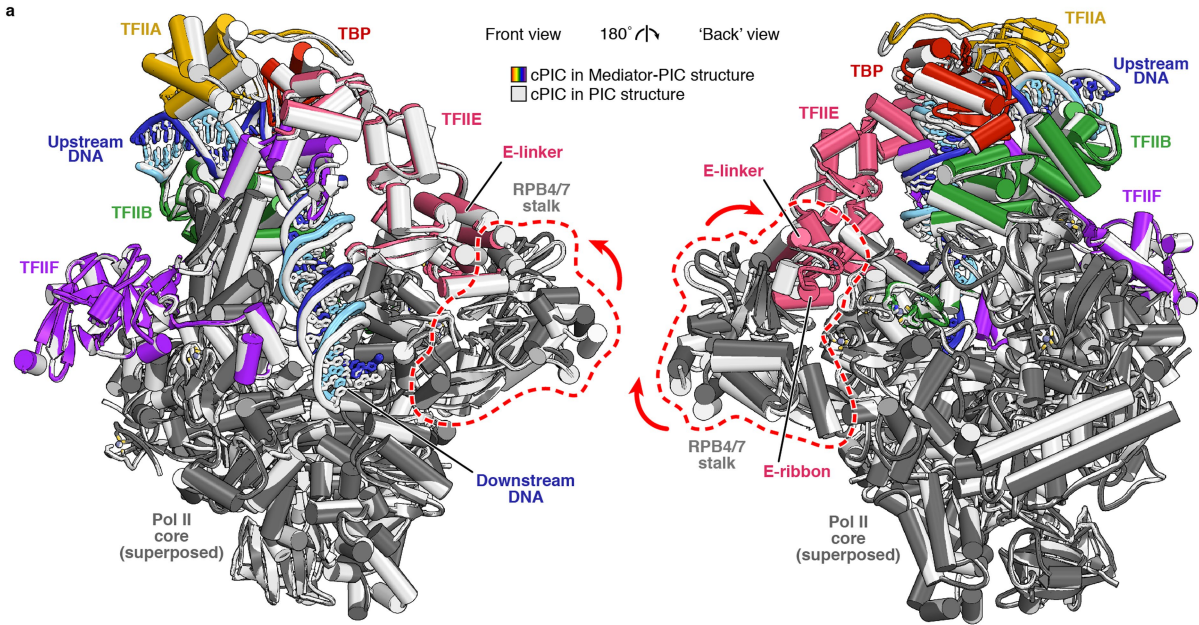


Extended Data Fig. 3 | FSCs of reconstructions and cryo-EM density.
a, Solvent-corrected 'gold-standard' FSCs for the reconstructions shown in Extended Data Fig. 2c. Unmasked (green), masked (blue), and phase-randomized (red) FSCs are also shown. **b**, Schematic representation of Mediator subunit domain architecture. Regions contributing to submodules are coloured according to the *S. pombe* cMed structure²³. Unassigned regions

are coloured grey. **c**, Local-resolution-filtered map of Mediator-PIC with the fitted structure. The inset shows a magnified view of the CAK module fitting into our density. **d**, Model-to-map FSCs, showing in blue the fit of the overall structure to the Mediator-PIC and in black the fit of the Mediator-Pol II stalk model to their corresponding maps.



Extended Data Fig. 4 | Quality of cryo-EM densities. Sections of focused-refined Mediator–stalk cryo-EM density overlaid with their respective atomic models. Densities are shown as a blue mesh, and sticks are shown for the model coloured as in Extended Fig. 3c.



Extended Data Fig. 5 | Additional structural comparisons. **a**, Comparison of the human Mediator–PIC structure (this study) with the free PIC structure²⁵ reveals a different orientation of the Pol II RPB4–RPB7 stalk. The core PIC regions of the Mediator–PIC (in colour) and free PIC (in white) structures were superposed on the 10-subunit Pol II core. Mobile elements in the stalk are indicated and conformational changes between complexes are depicted by red

arrows. **b**, Comparison of the yeast and human Mediator–PIC structures reveals a different relative orientation of the Mediator middle module. The human (in colour) and yeast⁹ (in white) Mediator–PIC structures were superposed on the well-conserved neck and fixed-jaw domains of the Mediator head module. Conformational changes of Mediator submodules are depicted by red arrows. The proximal tail region of human Mediator was omitted for clarity.

Article

Extended Data Table 1 | Cryo-EM data collection and processing

| Sample | Mediator-PIC | | |
|---------------------------------------|--------------------------------------|-----------------------|------------------|
| Data acquisition | | | |
| Voltage | 300 kV | | |
| Magnification | 81,000 | | |
| Pixel size | 1.05 Å | | |
| Electron dose | 58.56 e ⁻ /Å ² | | |
| Frame number | 40 | | |
| Defocus range | 0.3-5.0 | | |
| Data Processing | | | |
| | Mediator-PIC | Mediator-Pol II stalk | TFIIH |
| EMDB code | 12610 | 12609 | |
| PDB code | 7NVR | | |
| Final number of particles | 25,967 | 85,182 | 83,713 |
| Map resolution at 0.143 FSC | 4.5 Å | 4.0 Å | 6.5 Å |
| Local resolution range | 4.0 – 15.0 Å | 3.5 – 11.5 Å | 5.5 – 13.5 Å |
| Map sharpening B-factor | -80 Å ² | -80 Å ² | 0 Å ² |
| Model composition | | | |
| Initial PDB used | 7NVS | | |
| No. of atoms | 96,180 | | |
| Protein | 11,548 | | |
| DNA | 128 | | |
| Ligand | Zn: 18 Mg: 1 SF4: 1 UNK:137 | | |
| Mean B factors (Å²) | | | |
| Protein | 111.2 | | |
| Nucleotides | 110.3 | | |
| Ligand | 142.6 | | |
| Model validation | | | |
| MolProbity score | 1.72 | | |
| Clash score | 8.39 | | |
| Rotamer outliers (%) | 0.01 | | |
| C-beta outliers | 0.00 | | |
| Ramachandran plot | | | |
| Favored | 96.05 | | |
| Allowed | 3.93 | | |
| Outliers | 0.03 | | |

Reporting Summary

Nature Research wishes to improve the reproducibility of the work that we publish. This form provides structure for consistency and transparency in reporting. For further information on Nature Research policies, see our [Editorial Policies](#) and the [Editorial Policy Checklist](#).

Statistics

For all statistical analyses, confirm that the following items are present in the figure legend, table legend, main text, or Methods section.

n/a Confirmed

- | | | |
|-------------------------------------|-------------------------------------|------------------------------------------------------------------------------------------------------------------------------------------------------------------------------------------------------------------------------------------------------------|
| <input type="checkbox"/> | <input checked="" type="checkbox"/> | The exact sample size (n) for each experimental group/condition, given as a discrete number and unit of measurement |
| <input type="checkbox"/> | <input checked="" type="checkbox"/> | A statement on whether measurements were taken from distinct samples or whether the same sample was measured repeatedly |
| <input type="checkbox"/> | <input checked="" type="checkbox"/> | The statistical test(s) used AND whether they are one- or two-sided <i>Only common tests should be described solely by name; describe more complex techniques in the Methods section.</i> |
| <input type="checkbox"/> | <input checked="" type="checkbox"/> | A description of all covariates tested |
| <input type="checkbox"/> | <input checked="" type="checkbox"/> | A description of any assumptions or corrections, such as tests of normality and adjustment for multiple comparisons |
| <input type="checkbox"/> | <input checked="" type="checkbox"/> | A full description of the statistical parameters including central tendency (e.g. means) or other basic estimates (e.g. regression coefficient) AND variation (e.g. standard deviation) or associated estimates of uncertainty (e.g. confidence intervals) |
| <input type="checkbox"/> | <input checked="" type="checkbox"/> | For null hypothesis testing, the test statistic (e.g. F , t , r) with confidence intervals, effect sizes, degrees of freedom and P value noted <i>Give P values as exact values whenever suitable.</i> |
| <input checked="" type="checkbox"/> | <input type="checkbox"/> | For Bayesian analysis, information on the choice of priors and Markov chain Monte Carlo settings |
| <input checked="" type="checkbox"/> | <input type="checkbox"/> | For hierarchical and complex designs, identification of the appropriate level for tests and full reporting of outcomes |
| <input checked="" type="checkbox"/> | <input type="checkbox"/> | Estimates of effect sizes (e.g. Cohen's d , Pearson's r), indicating how they were calculated |

Our web collection on [statistics for biologists](#) contains articles on many of the points above.

Software and code

Policy information about [availability of computer code](#)

Data collection Serial EM 3.8 beta 8

Data analysis RELION 3.1.0, UCSF Chimera 1.13, UCSF ChimeraX v1.11, Pymol 2.3.4, Coot 0.8.9.2, Warp v1.0.7-1.0.9, PHENIX 1.18.2, cryoSPARC 2.14.2, Molprobity 4.5, T-Coffee Espresso

For manuscripts utilizing custom algorithms or software that are central to the research but not yet described in published literature, software must be made available to editors and reviewers. We strongly encourage code deposition in a community repository (e.g. GitHub). See the Nature Research [guidelines for submitting code & software](#) for further information.

Data

Policy information about [availability of data](#)

All manuscripts must include a [data availability statement](#). This statement should provide the following information, where applicable:

- Accession codes, unique identifiers, or web links for publicly available datasets
- A list of figures that have associated raw data
- A description of any restrictions on data availability

The cryo-EM density reconstructions and final models were deposited with the EMDB (EMD-12609) for Mediator + Pol II Stalk and EMD-12610 for Mediator + PIC) and with the PDB (7NVR). All data is available in the main text or the supplementary materials.

Field-specific reporting

Please select the one below that is the best fit for your research. If you are not sure, read the appropriate sections before making your selection.

Life sciences Behavioural & social sciences Ecological, evolutionary & environmental sciences

For a reference copy of the document with all sections, see [nature.com/documents/nr-reporting-summary-flat.pdf](https://www.nature.com/documents/nr-reporting-summary-flat.pdf)

Life sciences study design

All studies must disclose on these points even when the disclosure is negative.

| | |
|-----------------|---------------------------------------------------------------------------------------------------------------------------------------------------------------------------------------------------------------------------------------------------------------------------------------------------------------------------------------------------------------------------------------------------------------------------------------------------------------------------------------------------------------------------------------------------------------------------------------------------------------|
| Sample size | No Sample size calculations were performed. For cryo-EM samples, eleven grids of Mediator-PIC sample were pre-screened to identify the optimal grid for data collection. The number of grids screened were random and was not limited by any experimental parameter. Biochemical experiments were performed with three sample replicates and each experiment was repeated minimum thrice. This is a standard in the field and the sample size was sufficient to observe the effect and binary outcome of this experiment. i.e. Mediator stimulation of Pol II CTD phosphorylation processing by western blot. |
| Data exclusions | No data were excluded from the analyses. |
| Replication | All attempts at replication were successful. The kinase assay and western blot experiments were repeated minimum thrice. Cryo-EM single particle analysis inherently relies on averaging over a large number of independent observations. During the processing pipeline, replicate reconstructions were calculated over 3 times during the polishing and other related refinement procedures, yielding the same results at different resolutions. |
| Randomization | Samples were not allocated to groups. All cryo-EM particles used for structure determination adopt random orientations in ice on the grid. Division of particles into random halves is automatically performed during 3D reconstruction by Relion 3.1.0. Other experiments did not involve randomization. |
| Blinding | Blinding is not applicable for this study, as group allocation is not used. |

Reporting for specific materials, systems and methods

We require information from authors about some types of materials, experimental systems and methods used in many studies. Here, indicate whether each material, system or method listed is relevant to your study. If you are not sure if a list item applies to your research, read the appropriate section before selecting a response.

Materials & experimental systems

| n/a | Involvement in the study |
|-------------------------------------|-----------------------------------------------------------|
| <input type="checkbox"/> | <input checked="" type="checkbox"/> Antibodies |
| <input type="checkbox"/> | <input checked="" type="checkbox"/> Eukaryotic cell lines |
| <input checked="" type="checkbox"/> | <input type="checkbox"/> Palaeontology and archaeology |
| <input checked="" type="checkbox"/> | <input type="checkbox"/> Animals and other organisms |
| <input checked="" type="checkbox"/> | <input type="checkbox"/> Human research participants |
| <input checked="" type="checkbox"/> | <input type="checkbox"/> Clinical data |
| <input checked="" type="checkbox"/> | <input type="checkbox"/> Dual use research of concern |

Methods

| n/a | Involvement in the study |
|-------------------------------------|-------------------------------------------------|
| <input checked="" type="checkbox"/> | <input type="checkbox"/> ChIP-seq |
| <input checked="" type="checkbox"/> | <input type="checkbox"/> Flow cytometry |
| <input checked="" type="checkbox"/> | <input type="checkbox"/> MRI-based neuroimaging |

Antibodies

| | |
|-----------------|-------------------------------------------------------------------------------------------------------------------------------------------------------------------------------------------------------------------------------------------------------------------------------------------------------------------------------------------------------------------------------------------------|
| Antibodies used | Primary antibodies used were: Pol II CTD Ser5 phosphorylation rat clone 3E8 Ab (1:2000, Sigma Aldrich-#04-1572-I), RPB3 rabbit polyclonal Ab (1:2000 dilution, Bethyl Laboratories Inc-#A303-771A). The secondary antibodies used were: HRP-conjugated anti-rat secondary antibody (1:5000, Sigma-Aldrich-#A9037) and HRP conjugated anti-rabbit (1:5000, GE Healthcare Life Sciences-#NA934) |
| Validation | The antibodies used in study has been evaluated in our group in previously peer-reviewed publications or by other groups in peer-reviewed publications. Pol II ser 5 phospho 3E8 antibody (Vos S et al, 2018 Nature); RPB3 rabbit polyclonal Ab (Dubbury et al, 2018 Nature) |

Eukaryotic cell lines

Policy information about [cell lines](#)

| | |
|---------------------|------------------------------------------------------------------------------------------------------------------------------------------------------------------------------------------------------------------------------------------------------|
| Cell line source(s) | Hi5 cells: Expression Systems, Tni Insect cells in ESF921 media, item 94-002F Sf9 cells: ThermoFisher, Catalogue Number 12659017, Sf9 cells in Sf-9000TM III SFM Sf21 cells: Expression Systems, Sf21 insect cells in ESF921 medium, Item 94-003F |
|---------------------|------------------------------------------------------------------------------------------------------------------------------------------------------------------------------------------------------------------------------------------------------|

Authentication

Isozyme and karyotype analysis by commercial supplier (ThermoFisher and Expression Systems). Cell lines were not authenticated in-house.

Mycoplasma contamination

Cell lines were not tested for mycoplasma contamination.

Commonly misidentified lines
(See [ICLAC](#) register)

No commonly misidentified cell lines were used.